



# Ultrathin dodecyl-sulfate-intercalated Mg-Al layered double hydroxide nanosheets with high adsorption capability for dye pollution

Siqi Lei<sup>a</sup>, Sinong Wang<sup>b,\*</sup>, Boxu Gao<sup>c</sup>, Yulu Zhan<sup>c</sup>, Qiancheng Zhao<sup>c</sup>, Shanshan Jin<sup>b</sup>, Guoxin Song<sup>a</sup>, Xinchun Lyu<sup>a,\*</sup>, Yahong Zhang<sup>c</sup>, Yi Tang<sup>c,\*</sup>

<sup>a</sup> Research Center for Analysis and Measurement, Fudan University, Shanghai 200433, PR China

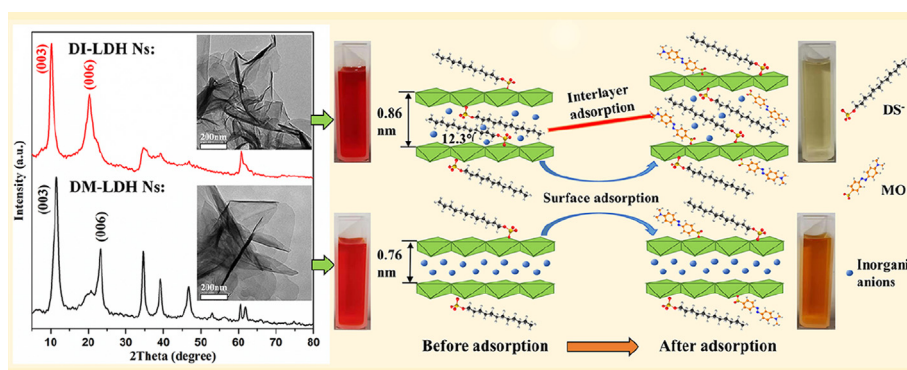
<sup>b</sup> Institute for Preservation of Chinese Ancient Books, Fudan University Library, Fudan University, Shanghai 200433, PR China

<sup>c</sup> Department of Chemistry, Shanghai Key Laboratory of Molecular Catalysis and Innovative Materials, Collaborative Innovation Centre of Chemistry for Energy Materials, Fudan University, Shanghai 200433, PR China

## HIGHLIGHTS

- The dodecyl-sulfate-intercalated Mg-Al-LDH nanosheets with ultrathin morphology are synthesized for solving dye pollution.
- This simple one-step surfactant-assisted synthetic method avoids the strict conditions to prevent  $\text{CO}_3^{2-}$  pollution.
- The LDH adsorbs methyl orange from aqueous solution effectively and rapidly.
- The surface-interlayer-adsorption mechanism is proposed for its high dye-removal performance.

## GRAPHICAL ABSTRACT



## ARTICLE INFO

### Article history:

Received 1 March 2020

Revised 12 May 2020

Accepted 14 May 2020

Available online 20 May 2020

### Keywords:

Layered double hydroxide

One-step synthesis

Intercalation

Ultrathin

Adsorption

Methyl orange

Adsorption mechanism

## ABSTRACT

A high-performance dye adsorbent of ultrathin dodecyl-sulfate ( $\text{DS}^-$ ) intercalated Mg-Al layered double hydroxide nanosheets (DI-LDH Ns) were controllably synthesized by a simple one-step surfactant-assisted hydrothermal method. The unique intercalated structure with weak interlayer interaction and high accessible surface of DI-LDH Ns provide efficient adsorption of methyl orange (MO), leading to its superior performance with much higher uptake capability (846.6 mg/g at 298 K) and less adsorbing equilibrium time (5 min) than those of ultrathin  $\text{DS}^-$ -surface-modified Mg-Al-LDH nanosheets (DM-LDH Ns, 327.4 mg/g at 298 K, 120 min) and original Mg-Al-LDH (O-LDH, 208.2 mg/g at 298 K, 120 min). The composition and structure of these LDHs were investigated by systematic physicochemical characterization, such as XRD, TEM, FT-IR, BET and TGA. The adsorption behavior of DI-LDH Ns follows the Langmuir isotherm equation. A plausible mechanism is proposed to explain the adsorption process of such DI-LDH Ns, in which the synergistic contributions of surface and interlayer adsorption between DI-LDH Ns and MO play an important role. This study puts forward a new thought for the development of high-performance LDH adsorbents with an ultrathin intercalated structure for the efficient and rapid removal of dyes.

© 2020 Elsevier Inc. All rights reserved.

\* Corresponding authors.

E-mail addresses: [wangsn@fudan.edu.cn](mailto:wangsn@fudan.edu.cn) (S. Wang), [lvxinchun@fudan.edu.cn](mailto:lvxinchun@fudan.edu.cn) (X. Lyu), [yitang@fudan.edu.cn](mailto:yitang@fudan.edu.cn) (Y. Tang).

## 1. Introduction

Water pollution caused by dyestuff discharge from industrial processes has been a serious environmental challenge and crucial public health issue [1]. Dyes with stable chemical properties and structures are difficult to degrade under natural conditions, even in long-term treatment with oxidizing agents or biodegradation [2,3]. Although various technologies such as chemical redox, electrochemical treatment, ion exchange, and membrane process have been used for dyes removal [4], the adsorption method is considered as one of the most promising techniques due to its low-cost, easy-operation and high-efficiency [5]. Therefore, several materials, e.g. metal oxide [6], zeolite [7], and activated carbon [8], have attracted considerable attention as adsorbents in dye-removal applications. Notably, layered materials, which possess abundant flexible interlayer slit-pore with large potential surface area, are supposed to be an important type of adsorbents, such as graphene [9], boron nitride [10], and montmorillonite [4]. However, most layered adsorbents often suffer from either limited and sluggish adsorption performance due to the strong interaction between layers or cost-consuming and multi-step preparation processes.

Layered double hydroxides (LDHs) are a versatile kind of ionic lamellar materials, which can be expressed as  $[M_{1-y}^{2+}M_y^{3+}(\text{OH})_2]^{y+}(\text{A}^{n-})_{y/n}\cdot z\text{H}_2\text{O}$ , where  $M^{2+}$ ,  $M^{3+}$ , and  $A^{n-}$  represent the divalent cations, trivalent cations, and anions respectively [11]. Owing to their laminate structure, chemical multifunctionality, and interlayer ion-exchange property [12,13], LDHs have drawn wide attention in many fields, such as catalysts, supercapacitors, drug delivery as well as promising adsorbents for dye removal [14–17]. Many efforts have been made to improve the adsorption performance of conventional LDHs, such as modifying their surface with organic anions [18], preparing layered double oxides via calcination [19], and assembling graphene for cumulating their adsorption characteristics [20]. In order to utilize the slit-like spaces between the layers of LDHs for enhancing their adsorption capability, the post-synthesis techniques have been adopted to exchange organic or inorganic anions into their interspace. However, the anion-exchange strategy often suffers from the complex multi-step process with poor product crystallinity and low exchange efficiency, making obtained products unsatisfactory in practical application [21]. And the roasting recovery method, another post-synthesis method with the multi-step process, could achieve high exchange efficiency, but the roasting operation would inevitably influence the crystallinity of host hydroxide sheets [22]. Although the co-precipitation method might greatly facilitate the one-step preparation of intercalated LDHs, the prepared products are often with poor crystallinity and small specific surface area [18,23]. What is worse, the above methods require strict synthetic conditions with air isolation and water purification to ensure that  $\text{CO}_3^{2-}$  cannot intercalate into the lamellae of LDHs due to its much higher affinity than other intercalated anions [24]. Furthermore, the preparation of ultrathin LDHs with larger surface area is another strategy to improve LDHs' performance for pollution adsorption. However, to our best knowledge, few works have been done for preparing intercalated LDHs with ultrathin morphology in this field. Therefore, an easy and effective strategy for the controllable preparation of organic-molecule-intercalated ultrathin LDH nanosheets is highly desired for adsorbing dye contaminants.

In this work, a one-step hydrothermal method has been developed to prepare ultrathin Mg-Al-LDHs with tunable surfactant-intercalated structure. Utilizing sodium dodecyl sulfate (SDS) as the structure-direct agent and intercalated component, the ultrathin dodecyl-sulfate ( $\text{DS}^-$ ) intercalated Mg-Al-LDH nanosheets (DI-LDH Ns) and the ultrathin  $\text{DS}^-$ -surface-modified Mg-Al-LDH nanosheets (DM-LDH Ns) can be simply synthesized by adjusting the adding amount of SDS. As an example, methyl orange (MO), a

highly deleterious and commonly used dye in industry [25], is adopted to investigate the adsorption capability of DI-LDH Ns and DM-LDH Ns for dye pollution. Such DI-LDH Ns is expected to exhibit high uptake capability and fast adsorbing velocity due to its unique  $\text{DS}^-$ -intercalated structure and high accessible  $\text{DS}^-$ -modified surface with the affinity for organic dyes [26]. Significantly, a surface-interlayer-adsorption mechanism is proposed to explain its high dye-removal performance, which depends on the synergistic contributions of surface and interlayer adsorption between DI-LDH Ns and dyes.

## 2. Experimental section

### 2.1. Materials and reagents

Magnesium nitrate hexahydrate ( $\text{Mg}(\text{NO}_3)_2\cdot 6\text{H}_2\text{O}$ ), aluminum nitrate nonahydrate ( $\text{Al}(\text{NO}_3)_3\cdot 9\text{H}_2\text{O}$ ), hexamethylenetetramine (HMT,  $\text{C}_6\text{H}_{12}\text{N}_4$ ) and absolute ethanol ( $\text{C}_2\text{H}_6\text{O}$ ) were of analytical grade. Sodium dodecyl sulfate (SDS,  $\text{C}_{12}\text{H}_{25}\text{NaO}_4\text{S}$ ) was of chemical-pure grade. And the above chemicals were all purchased from Sinopharm Chemical Reagent Co., Ltd. (Shanghai, China). Methyl orange (MO,  $\text{C}_{14}\text{H}_{14}\text{N}_3\text{SO}_3\text{Na}$ , 96 wt%) was used as an adsorbate and applied by Shanghai Aladdin Bio-Chem Technology Co., Ltd (Shanghai, China). Deionized water (18  $\text{M}\Omega\cdot\text{cm}$ ) was used throughout the process.

### 2.2. Preparation of ultrathin Mg-Al-LDH nanosheets

The one-step surfactant-assisted hydrothermal method is described as follows: 0.01 mol  $\text{Mg}(\text{NO}_3)_2\cdot 6\text{H}_2\text{O}$ , 0.005 mol  $\text{Al}(\text{NO}_3)_3\cdot 9\text{H}_2\text{O}$ , 0.013 mol HMT, and SDS were dissolved respectively in total 40 mL deionized water and mixed simultaneously. The amount of SDS was added referring to  $\text{SDS}/(\text{Mg}^{2+}+\text{Al}^{3+}) = 0.173\text{--}0.347$  (mole ratio). After continuously stirred for a few minutes at room temperature, the mixture turned into white viscous liquid. Then the mixture was poured into a 100 mL Teflon vessel, sealed in a stainless-steel vessel and heated at 140 °C for 24 h to crystallize well. The obtained sediment was collected by centrifugation at 4000 rpm/min and washed firstly with absolute ethanol then deionized water for several times. Finally, freeze-dried technology was utilized to dry the products.

### 2.3. Adsorption experiments

All the adsorption experiments were carried out in 100 mL plastic centrifugal tubes which contain 50 mL MO solution and 0.1 g adsorbent. Initial concentrations of MO aqueous solutions ranged from 100 mg/L to 2000 mg/L. Ultrathin Mg-Al LDH nanosheets were utilized without dried in adsorption treatment, and the solid content of undried adsorbents was determined by three parallel drying experiments. The mixtures of MO solution and adsorbent were treated with a 30-second supersonic oscillation and then gently stirred 24 h at a specific pH value. This reaction time is far longer than the equilibrium time measured by preliminary tests to make sure adequate interaction between MO and adsorbents. The pH values of solutions were adjusted by 1 M HCl or NaOH. Besides, ultrasonic treatment was not performed on the investigations of the effect of contact time. After adsorption, 3 mL mixture was extracted by a disposable syringe and filtered by a 0.45  $\mu\text{m}$  Millipore filter. The concentrations of filtered solutions were analyzed by an ultraviolet-visible (UV-Vis) spectrophotometer at the wavelength of 464 nm. The effect of time was investigated by collecting solution samples at pre-set time interval. The effect of pH was investigated within the pH range of 6.0–11.0. And the

effect of temperature was also discussed according to the trials under 298, 303, 308 and 313 K, respectively.

#### 2.4. Characterization

X-ray diffraction (XRD) patterns of samples were measured by a Bruker D2-Phaser X-ray diffractometer (Cu  $K\alpha$  radiation,  $\lambda = 0.15418$  nm) at the  $2\theta$  range of  $2^\circ$ – $80^\circ$ . Transmission electron microscope (TEM) images were obtained by a Jeol JEM-2011 at the energy of 200 kV. Fourier transform infrared spectroscopy (FT-IR) spectra were obtained by a PerkinElmer Spectrum Two FT-IR spectrometer in the wavenumber range of  $450$ – $4000$   $\text{cm}^{-1}$ . And the  $\text{N}_2$  adsorption–desorption measurements were operated on a Quantachrome Autosorb IQ2 auto-gas sorption analyzer. Zeta potential data were obtained with a Malvern ZEN3690. Thermogravimetric analysis (TGA) was carried out on a PerkinElmer TGA-8000 in the temperature range of  $30$ – $700$   $^\circ\text{C}$  with a heating rate of  $10$   $^\circ\text{C}/\text{min}$  under the air atmosphere. The pH values were determined by a Leici PHSJ-6L equipped with a Leici E-201-P planar composite pH electrode. To investigate the concentrations of dye solutions, UV–Vis absorption spectrometry was applied with a PerkinElmer PE-Lambda spectrophotometer.

### 3. Results and discussion

#### 3.1. Characterization of ultrathin Mg–Al–LDH nanosheets

A series of Mg–Al–LDH nanosheets were prepared by one-step hydrothermal method with the assistance of SDS, and the products were denoted as L1 (DM-LDH Ns), L2, L3 and L4 (DI-LDH Ns) in the systems which the molar ratio of  $\text{SDS}/(\text{Mg}^{2+} + \text{Al}^{3+})$  was 0.173, 0.260, 0.303 and 0.347, respectively. A sample of pure original Mg–Al–LDH (L0, O-LDH) was also prepared under the same condition merely without adding SDS. Their tunable crystalline structures were characterized by XRD (Fig. 1). The XRD pattern with characteristic (0 0  $l$ ) basal reflections confirms L0 as  $\text{CO}_3^{2-}$ -intercalated Mg–Al–LDH (JCPDS no. 70–2151) with quite well crystallinity and the typical layer spacing of  $d = 0.76$  nm [18,22]. The (0 0 3) and (0 0 6) reflections at  $11.56^\circ$  and  $23.01^\circ$  appear in the patterns of L1 and L2 samples, indicating they retain the typical structure of  $\text{CO}_3^{2-}$ -intercalated LDHs. The obvious broadening of diffraction peaks from L0 to L2 is probably attributed to the restriction effect of adsorbed  $\text{DS}^-$  anions on the growth of LDH crystal along [0 0 1] direction due to the relatively strong interaction between them. With the SDS content increases, new reflections at  $10.17^\circ$  and  $20.35^\circ$  appear in the XRD patterns of L3 and L4. Meanwhile, the original characteristic diffraction peaks of  $\text{CO}_3^{2-}$ -intercalation vanish completely, indicating L4 as a novel  $\text{DS}^-$ -intercalated Mg–Al–LDH with the larger interlayer spacing of  $d = 0.86$  nm. Theoretical calculation of the layer distance of intercalated LDH should comprehensively considerate the size of intercalated anions, the thickness of hydroxide sheets, and the orientation of interlayer anions [27,28]. The chain length of all-*trans*  $\text{DS}^-$  is deduced to be  $1.78$  nm, and the thickness of metal hydroxide layers is  $0.48$  nm. Therefore, the tilt angle of interlayer surfactant is found to be  $12.3^\circ$  as illustrated in the upper inset of Fig. 1 [22,24,27]. Moreover, all the samples with the (1 1 0) reflection provide the evidence that they remain intact hydroxide sheets of LDH with the surfactant assistance. However, the (0 1 2), (0 1 5) and (0 1 8) peaks gradually weaken and widen from L0 to L4, demonstrating the decrease of stacking order of LDH layers or the thinness of LDH nanosheets at [0 0 1] direction with the increasing SDS addition.

L1 and L4 were chosen as the representative models of DM-LDH Ns and DI-LDH Ns for the following characterizations and experi-

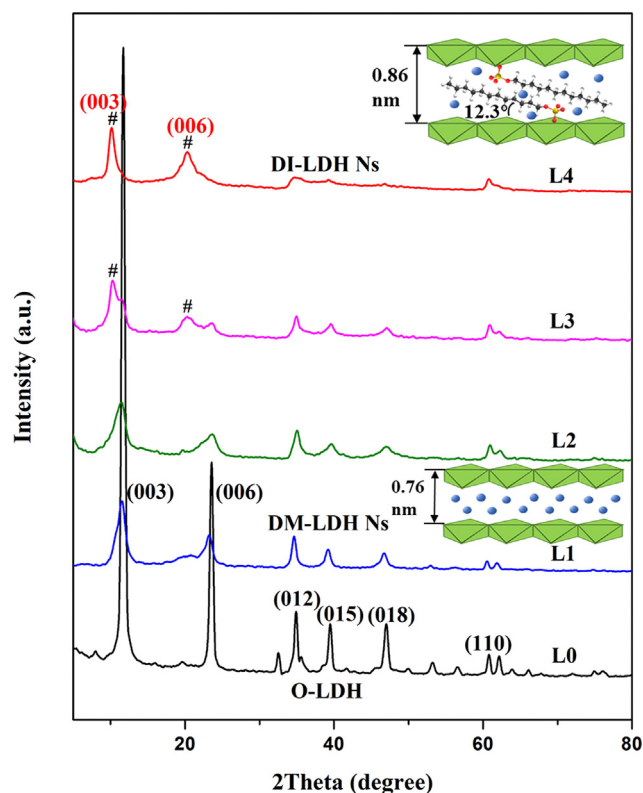


Fig. 1. XRD patterns of O-LDH and ultrathin Mg–Al–LDH nanosheets. The insets are structure diagrams of DI-LDH Ns and DM-LDH Ns, respectively.

ments. TEM images display the ultrathin nanosheets with the thickness about 7–20 nm of DI-LDH Ns (Fig. 2a, b) and 7–25 nm of DM-LDH Ns (Fig. 2c, d). It consists with the data calculated by the Debye–Scherrer formula based on their XRD patterns (Fig. 1), which shows that the thickness of DM-LDH Ns and DI-LDH Ns along [0 0 1] direction are averagely about 11.4 nm (*ca.* 15 layers) and 12.3 nm (*ca.* 14 layers), respectively, much thinner than that of O-LDH (Fig. 2e, f) with the size around 60.8 nm (*ca.* 80 layers). The nanosheet diameter of DM-LDH Ns is larger than that of DI-LDH Ns, suggesting that the addition of SDS not only refrains the growth of the (0 0 1) plane along the  $c$  axis of LDH but also limits that of (1 1 0) plane. Moreover, nanosheets observed in DI-LDH Ns exhibit the slightly curly morphology, which might be contributed to their thin and intercalated structure with flexible organic molecules between host layers.

Moreover, FT-IR spectroscopy was applied to study the vibration information of intercalated anions, hydroxyl groups and lattice [29,30]. As shown in Fig. 3a, the sharp absorption peaks of  $\text{C}=\text{O}$  band at  $1355$   $\text{cm}^{-1}$  in the spectra of O-LDHs and DM-LDH Ns prove their  $\text{CO}_3^{2-}$ -intercalated structures, while the rather weak absorption bands at  $1355$  and  $1381$   $\text{cm}^{-1}$  confirm DI-LDH Ns with less  $\text{CO}_3^{2-}$  and  $\text{NO}_3^-$  intercalation [22]. Meanwhile, the  $\text{DS}^-$  anion is further detected by the characteristic vibrations of  $-\text{CH}_2-$  at  $2922$   $\text{cm}^{-1}$ ,  $2853$   $\text{cm}^{-1}$  and  $\text{S}=\text{O}$  at  $1216$   $\text{cm}^{-1}$  in the spectra of DM-LDH Ns and notably DI-LDH Ns, suggesting both nanosheets have been modified by  $\text{DS}^-$  anions [31]. Considering the results from XRD, the novel DI-LDH Ns exists as  $\text{DS}^-$  anions intercalated nanosheets with larger interlayer spacing, whereas DM-LDH Ns mainly retains the  $\text{CO}_3^{2-}$ -intercalated layered structure with SDS surfactant modified on its external surface. Additionally, the obvious shift of the  $-\text{OH}$  stretching absorption peak from  $3363$   $\text{cm}^{-1}$  in O-LDH and DM-LDH Ns to  $3467$   $\text{cm}^{-1}$  in DI-LDH Ns indicates the change of intercalation anions influences the state of physically

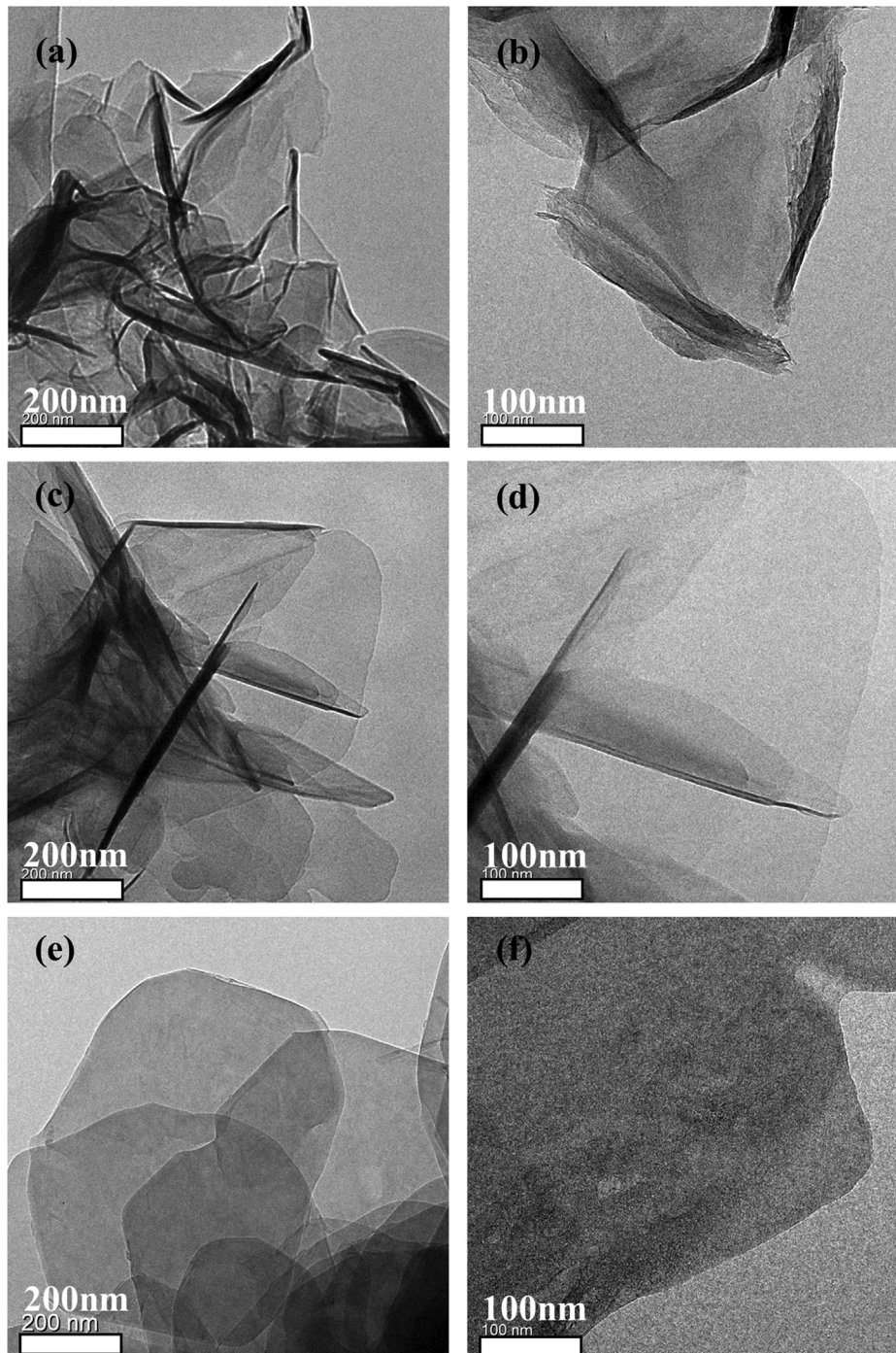


Fig. 2. TEM images of DI-LDH Ns (a, b), DM-LDH Ns (c, d) and O-LDH (e, f).

adsorbed water or the hydrogen bonds between the layers. The fingerprint area ( $450\text{--}900\text{ cm}^{-1}$ ) relates to the oxygen-metal-oxygen and metal-oxygen-metal stretching, and DI-LDH Ns also shows a different spectrum with O-LDH and DM-LDH Ns, probably resulting from the appearance of electrostatic attraction of the intercalated  $\text{DS}^-$  anions with LDH polycationic host layers in the former sample [19,32]. Meanwhile, the results calculated from  $\text{N}_2$  adsorption-desorption isotherm measurements (Fig. 3b, c, and S1, see supporting materials) show the Brunauer-Emmett-Teller (BET) surface area of 126.3, 96.6 and  $24.5\text{ m}^2/\text{g}$  for DI-LDH Ns, DM-LDH Ns, and O-LDH, respectively. The high surface area of DI-LDH Ns resulting from the ultrathin nanosheets morphology and  $\text{DS}^-$ -intercalated structure would promote its adsorption ability of dyes.

### 3.2. Adsorption behavior of ultrathin Mg-Al-LDH

#### 3.2.1. Effect of contact time

MO was used as an example to investigate the adsorption capability of DI-LDH Ns and DM-LDH Ns for dye pollution. Fig. 4 shows the amount of MO absorbed by the adsorbents with the change of time, namely  $q_t$  (mg/g), which can be calculated according to the mass balance equation [33].

$$q_t = \frac{(C_0 - C_t)V}{m} \quad (1)$$

Similarly, the adsorbing amount at equilibrium concentration ( $q_e$ , mg/g) can be obtained by:

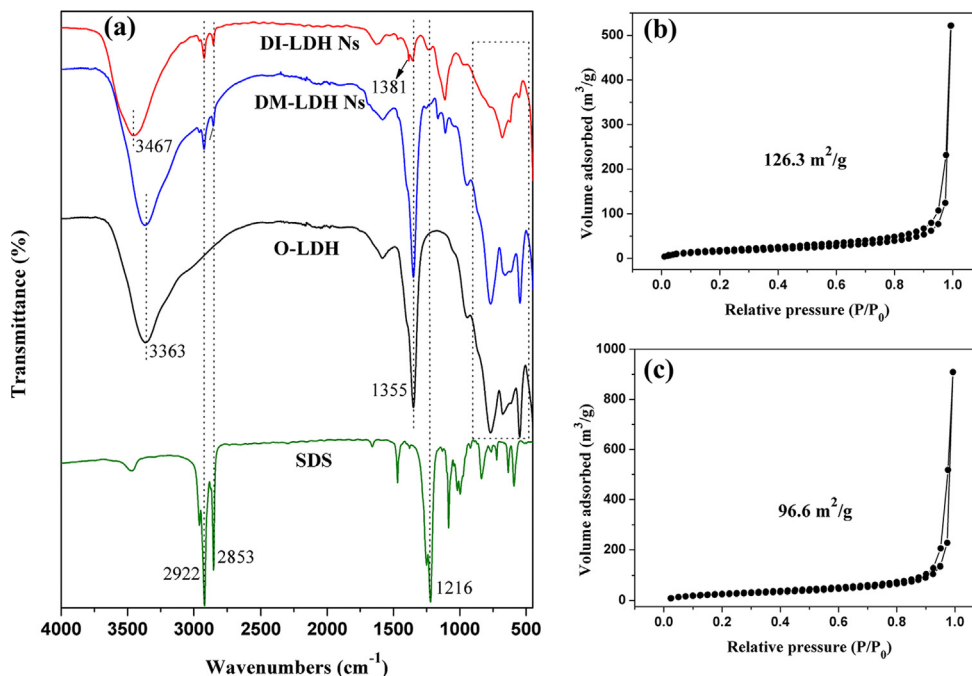


Fig. 3. FT-IR spectra of SDS, O-LDH, DM-LDH Ns and DI-LDH Ns (a).  $N_2$  adsorption/desorption isotherm of DI-LDH Ns (b) and DM-LDH Ns (c).

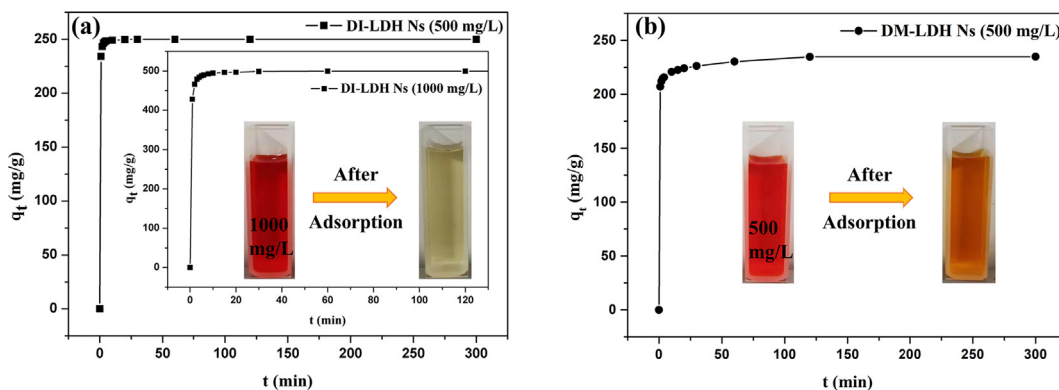


Fig. 4. Effect of contact time on MO adsorption amount at  $C_{0(MO)} = 500$  and 1000 (inset) mg/L for DI-LDH Ns (a), at  $C_{0(MO)} = 500$  mg/L for DM-LDH Ns (b),  $T = 298$  K,  $pH = 9.0$ ,  $m/V = 2$  g/L. Insets in (a) and (b) show the color change of MO solutions after adsorption treatment.

$$q_e = \frac{(C_0 - C_e)V}{m} \quad (2)$$

where  $C_0$ ,  $C_t$  and  $C_e$  (mg/L) represent the concentrations of dye solutions at the beginning, time of  $t$  (min), and equilibrium state, respectively.  $V$  (L) is the volume of solutions. And  $m$  (g) is the dried mass of adsorbents. The adsorption efficiency ( $E$ , %) is calculated as the following equation [33]:

$$E = (C_0 - C_e)/C_0 \times 100\% \quad (3)$$

In the experiment condition of 500 mg/L MO solution, DI-LDH Ns exhibits a rapid and thorough adsorption capability with the  $E$  value of 93.68% at the first minute. And its adsorption equilibrium state is reached in just 5 min with  $E$  of 99.44% (Fig. 4a, Table 1). While DM-LDH Ns realizes its  $E$  of 82.80% at the first minute and reaches its equilibrium state in 120 min with  $E$  of 93.88% (Fig. 4b, Table 2). The test of O-LDH adopts the MO concentration of 200 mg/L for its limited adsorption performance, the  $E$  is 75.90% at the first minute and the equilibrium time is 120 min with  $E$  of 97.50% (Fig. S2, Table S1). Comparing to O-LDH, DM-

LDH Ns exhibit more efficient performance in the initial stage of adsorption, while DI-LDH Ns not only expends much shorter time to reach its adsorption equilibrium but also realizes more thorough adsorption in treating dye polluted water. These distinct differences are attributed to the larger external surface area caused by ultrathin morphology or/and the interlayer adsorption due to the unique  $DS^-$ -intercalation structure which will be comprehensively discussed in Section 3.3. Owing to the rapid adsorption character of these two kinds of  $DS^-$ -containing ultrathin LDH nanosheets, it is hard to get enough points for kinetics analysis, but their high adsorption rates indicate that strong chemisorption takes place on them rather than physical adsorption [34]. Additionally, the outstanding capability of DI-LDH Ns is further verified in a higher MO concentration of 1000 mg/L (the inset of Fig. 4a, Table S2), showing its  $E$  value of 85.62% at the first minute and its equilibrium time of 10 min with  $E$  of 98.93%. And the UV-vis spectra (Fig S3) and photographs (Fig. 4) of samples after adsorption treatment clearly display the superior dye-removal capability of DI-LDH Ns comparing to DM-LDH Ns.

**Table 1**Effect of contact time on MO adsorption amount and efficiency at  $C_{0(MO)} = 500$  mg/L for DI-LDH Ns,  $T = 298$  K,  $pH = 9.0$ ,  $m/V = 2$  g/L.

$t$ (min)	1	2	3	4	5	10	20	30	60	120	300
$q_t$ (mg/g)	234.2	243.3	246.6	247.7	248.6	249.1	249.8	250.0	250.0	250.0	250.0
$E$ (%)	93.68	97.32	98.64	99.08	99.44	99.64	99.92	100.00	100.00	100.00	100.00

**Table 2**Effect of contact time on MO adsorption amount and efficiency at  $C_{0(MO)} = 500$  mg/L for DM-LDH Ns,  $T = 298$  K,  $pH = 9.0$ ,  $m/V = 2$  g/L.

$t$ (min)	1	2	3	4	10	15	20	30	60	120	300
$q_t$ (mg/g)	207.0	212.0	214.7	215.7	220.7	222.6	224.2	226.2	230.1	234.7	234.8
$E$ (%)	82.80	84.80	85.88	86.28	88.28	89.0	89.69	90.48	92.04	93.88	93.92

### 3.2.2. Effect of initial pH and temperature

The initial pH of adsorbate solution has an impact on the absorbing interaction by effecting zeta potential of adsorbents. Thus, the zeta potential of the LDHs is measured and presented in Fig. 5a. The values of DI-LDH Ns and DM-LDH Ns are very close to each other and lower than that of O-LDH, which could be ascribed to their similar properties of the external surface with the modification of the anionic surfactant. The MO adsorption capacity of DI-LDH Ns changing with the pH value shows a volcano curve with the maximum adsorption efficiency at  $pH = 9.0$  (Fig. 5b). The reason can be attributed to its unique  $DS^-$ -intercalated interlayer space and will be further explained in Section 3.3. Fig. 5c presents the adsorption behavior of DM-LDH

Ns with the increase of pH value, showing its sorption efficiency hardly alters in the pH range of 6.0–10.0 but sharply drops at the pH value of 11.0. The reason might be the negatively charged nanosheets would repulse MO anions and impede the adsorption process in a strong alkaline solution. Generally, both DI-LDH Ns and DM-LDH Ns adsorbents can be used in a wide pH range.

The trials were carried out at 298, 303, 308, and 313 K to figure out the effect of temperature on the MO adsorbing process (Fig. 5d, e). The result shows that the adsorption amount of DM-LDH Ns decreases as temperature rising, illustrating that an exothermic process takes place on it. On the contrary, the sorption capacity of DI-LDH Ns increases when the temperature increases. If we deduce that the external surface adsorbing of DI-LDH Ns is an

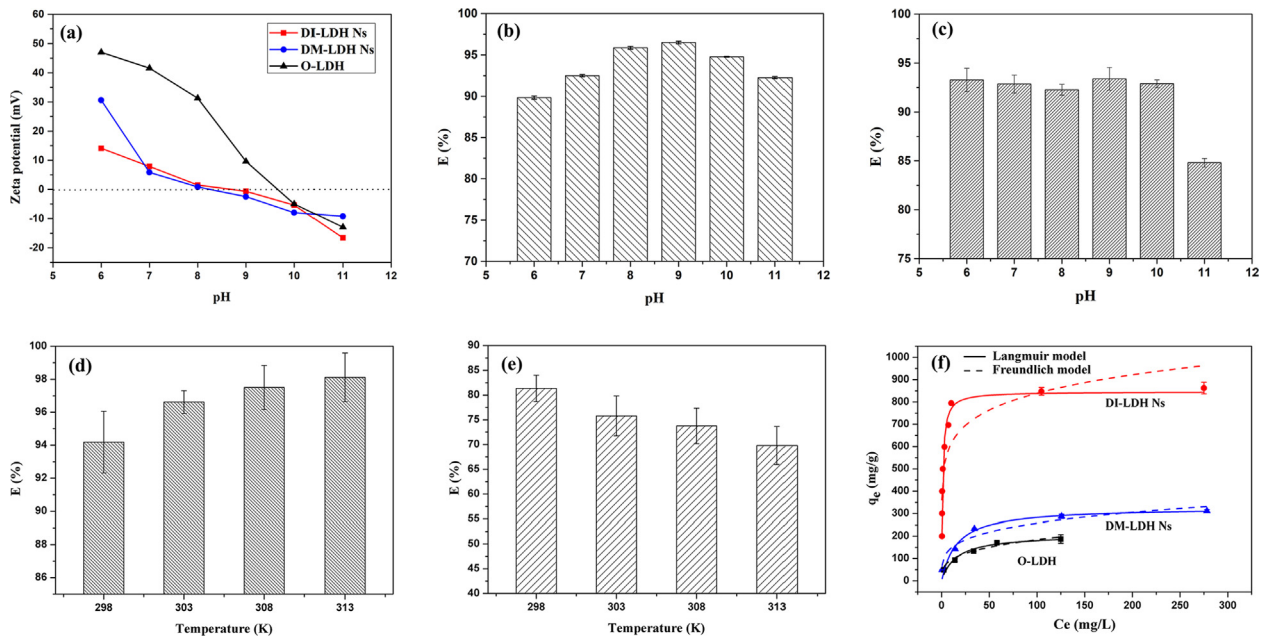


**Fig. 5.** Zeta potential of DI-LDH Ns, DM-LDH Ns and O-LDH at the pH range from 6.0 to 11.0 (a). Effect of pH on MO adsorption at  $T = 298$  K,  $C_{0(MO)} = 1800$  mg/L for DI-LDH Ns (b) and  $C_{0(MO)} = 500$  mg/L for DM-LDH Ns (c),  $pH = 6.0 \sim 11.0$ ,  $m/V = 2$  g/L, time = 24 h. Effect of temperature on MO adsorption at  $C_{0(MO)} = 1800$  mg/L for DI-LDH Ns (d) and  $C_{0(MO)} = 700$  mg/L for DM-LDH Ns (e),  $pH = 9.0$ ,  $m/V = 2$  g/L, time = 24 h,  $T = 298, 303, 308,$  and  $313$  K, respectively. Adsorption isotherm of MO on DI-LDH Ns, DM-LDH Ns and O-LDH at  $T = 298$  K,  $C_{0(MO)} = 100\text{--}2000$  mg/L,  $pH = 9.0$ ,  $m/V = 2$  g/L, time = 24 h (f).

**Table 3**

Isotherm parameters of Langmuir and Freundlich models for MO adsorption on DI-LDH Ns, DM-LDH Ns and O-LDH at 298 K.

Adsorbents	Freundlich model			Langmuir model				Amount of adsorption per unit of surface area ( $q_s$ , mg/m <sup>2</sup> )
	$K_F$ (mg <sup>1-n</sup> L <sup>n</sup> /g)	$n$	$R^2$	$q_{max}$ (mg/g)	$K_L$ (L/mg)	$R_L$	$R^2$	
DI-LDH Ns	47.982	0.292	0.721	846.6	1.001	0.003–0.001	0.963	6.70
DM-LDH Ns	83.865	0.244	0.929	327.4	0.063	0.074–0.016	0.948	3.39
O-LDH	448.800	0.135	0.936	208.2	0.065	0.133–0.030	0.937	8.51

exothermic process like DM-LDH Ns, the adsorption happening in interlayer space between hydroxide layers (seen in Section 3.3) should be an endothermic process, for higher temperature would facilitate the faster diffusion of MO molecules into the slit-pore. As a result, the absorption of MO on DI-LDH Ns displays an endothermic process apparently.

### 3.2.3. Adsorption isotherms

Adsorption isotherm plays a crucial role in analyzing the adsorption capacity of materials and providing information about solution-surface interaction. The sorption isotherm of MO on DI-LDH Ns, DM-LDH Ns and O-LDH at 298 K is shown in Fig. 5f. And two frequently used models, namely Langmuir and Freundlich isotherm models [35,36], are applied to isotherm fitting analysis. The Langmuir model can be described as the following formula:

$$q_e = \frac{K_L q_{max} C_e}{1 + K_L C_e} \quad (4)$$

where  $q_e$  and  $C_e$  were defined in Eq. (2);  $q_{max}$  (mg/g) is the maximum monolayer sorption capacity of adsorbents;  $K_L$  (L/mg) is a constant related to the adsorbing free energy. The Freundlich model can be represented as:

$$q_e = K_F C_e^n \quad (5)$$

where  $K_F$  ( $\text{mg}^{1-n}\text{L}^n/\text{g}$ ) and  $n$  are Freundlich constants, associating with sorption capacity and sorption intensity, respectively.

The fitting parameters and correlation coefficient values ( $R^2$ ) are all listed in Table 3. According to the  $R^2$  values, the more suitable model for all three kinds of LDH adsorbents is the Langmuir model, indicating the sorption processes are more likely to be homogeneous and monolayer. The obtained  $q_{max}$  values illustrate that the MO adsorbing capacity follows the order of DI-LDH Ns (846.6 mg/g) > DM-LDH Ns (327.4 mg/g) > O-LDH (208.2 mg/g). For the Langmuir model, a dimensionless constant named  $R_L$  can be calculated by the  $K_L$  constant to predict the favorability of this model.  $R_L$  could be obtained by the following equation [37]:

$$R_L = \frac{1}{1 + K_L C_0} \quad (6)$$

The value of  $R_L$  indicates that the Langmuir isotherm model is linear ( $R_L = 1$ ), favorable ( $0 < R_L < 1$ ), unfavorable ( $R_L > 1$ ), or irreversible ( $R_L = 0$ ) [38]. It is obvious that the resulting  $R_L$  values are in the range of 0–1, illustrating the Langmuir model is all favorable in the adsorption isotherm fitting of these Mg-Al-LDHs. From Table 4 in which lists the MO adsorption capacities of several materials and their applied conditions, it is found that DI-LDH Ns, with its shortest adsorption equilibrium time and highest adsorption capability, is a promising material in the real work of organic dye pollution treatment.

### 3.3. Adsorption mechanism

The adsorption mechanism was further studied by XRD, FT-IR and TGA characterization. As shown in Fig. 6a, the XRD pattern

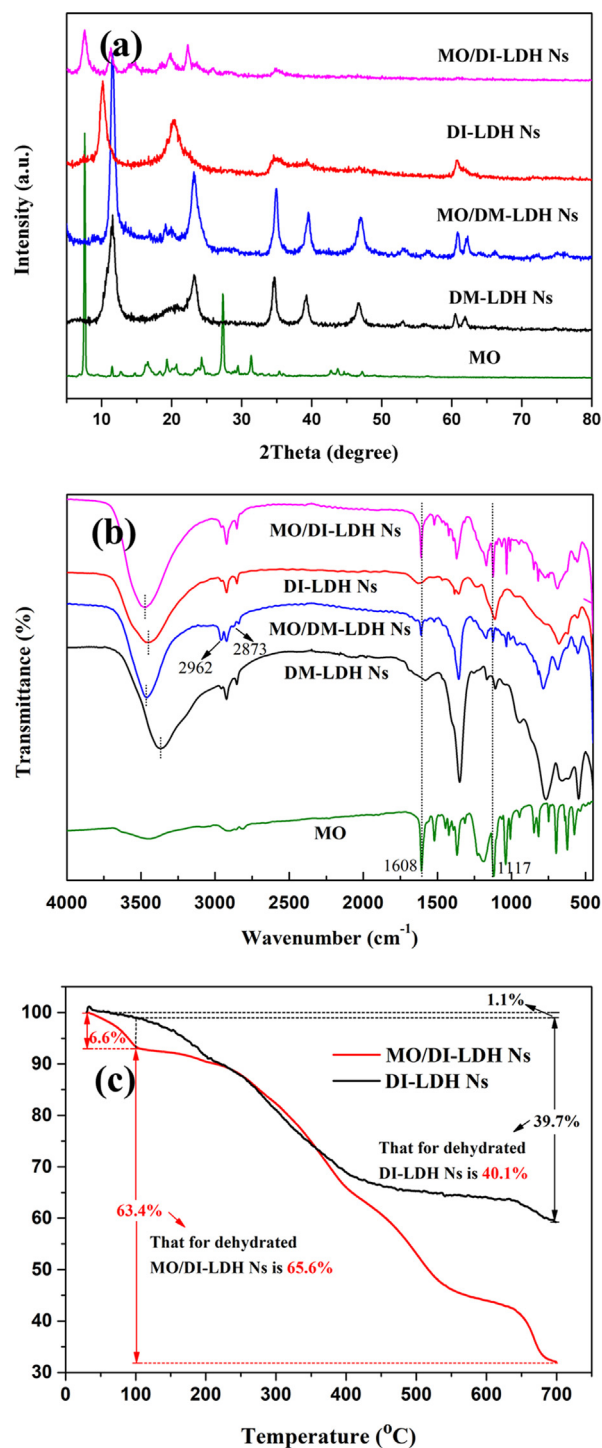


Fig. 6. XRD spectra (a) and FT-IR patterns (b) of MO, DM-LDH Ns and DI-LDH Ns before and after adsorption process. TGA thermograms (c) of DI-LDH Ns before and after adsorption process.

Table 4

Comparison of MO adsorption capacity with other adsorbents.

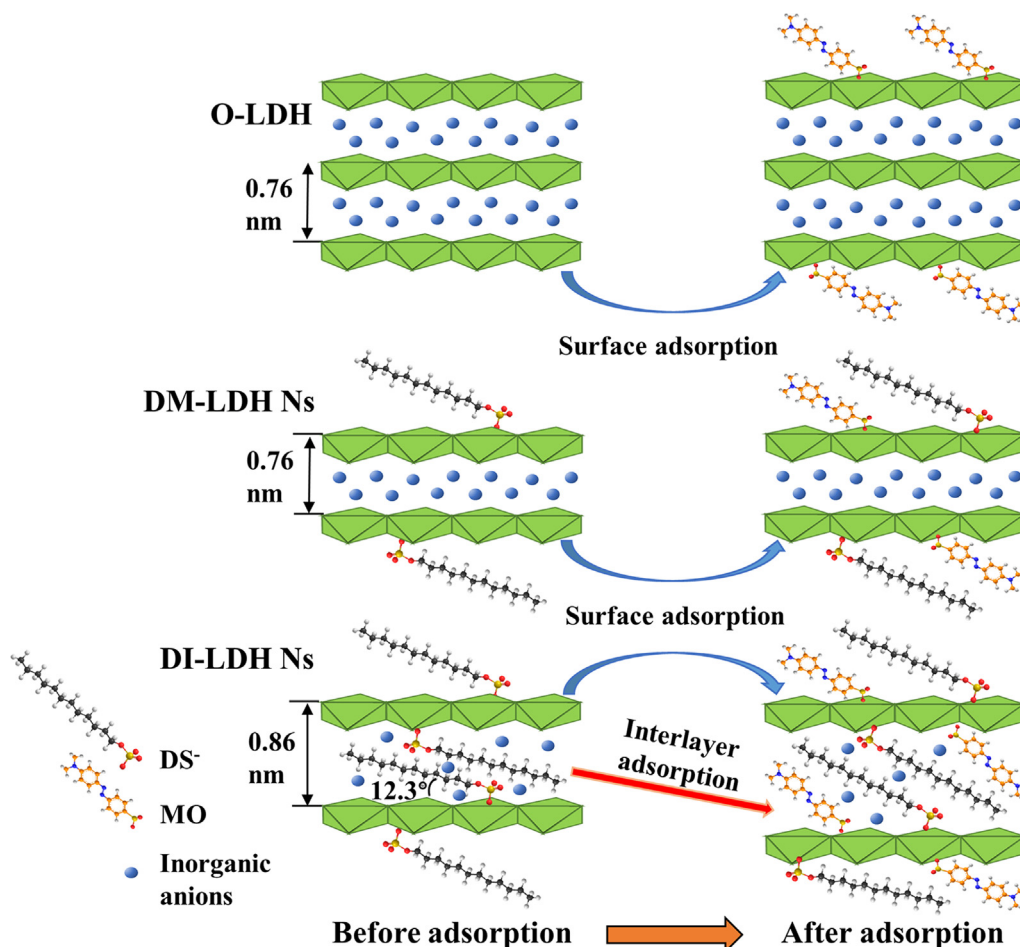
Adsorbents	Surface area (m <sup>2</sup> /g)	Adsorption condition				$q_{max}$ (mg/g)	Refs.
		pH	T (K)	t (min)	m/V (g/L)		
rGO/Ni/MMO	–	neutral	298	16 h	1	210.8	[5]
glycerol-modified LDH	71.4	4.5	298	30	0.1	443.5	[19]
RGO-Ni/Cr-CO <sub>3</sub> LDH	98.2	–	306	4 h	5	312.5	[39]
Fe <sub>3</sub> O <sub>4</sub> /ZnCr-LDH	185.2	6.4–7.3	385–415	35–59	0.05	240.16	[41]
flower-like-NiAl-LDH	133	3	298	100	1	500.6	[42]
DM-LDH Ns	96.6	9.0	298	2 h	2	327.4	This work
DI-LDH Ns	126.3	9.0	298	5	2	846.6	This work

of DI-LDH Ns after adsorption with MO (MO/DI-LDH Ns) is quite different from DI-LDH Ns itself with the new diffractions at  $3.36^\circ$  (see Fig S4) and  $7.66^\circ$  resulting from the increased interlayer distance, suggesting that the interlayer adsorption happens in DI-LDH Ns. While the XRD pattern of DM-LDH Ns after adsorption with MO (MO/DM-LDH Ns) has no change, suggesting the MO cannot enter the interlayer slit-pore of DM-LDH Ns and are mainly adsorbed on its external surface (Scheme 1). Considering the result of specific surface area of these two adsorbents (Fig. 3b, c) and the discrepancy of their MO adsorption amount (Fig. 5f), it is concluded that the interlayer adsorption of DI-LDH Ns is responsible to its much higher adsorption performance than that of DM-LDH Ns, in which its surfactant intercalated structure with weaker interlayer interaction plays a crucial role. FT-IR spectroscopy was also applied to study the interaction between adsorbents and MO. As shown in Fig. 6b, new bands appear in both MO/DI-LDH Ns and MO/DM-LDH Ns, and the most obvious bands at  $1608$  and  $1117\text{ cm}^{-1}$  are associated with the vibrations of phenyl groups and C–N in the MO molecule, respectively [39]. And the two peaks at  $2962$  and  $2873\text{ cm}^{-1}$  in MO/DM-LDH Ns, which belong to the asymmetric and symmetric vibrations of  $-\text{CH}_3$  [39], obviously strengthen than before, providing another proof of the adsorption of MO in DM-LDH Ns. It is also noticed that the characteristic peak of  $\text{NO}_3^-$  disappears after dye-adsorption treatment in the MO/DI-LDH Ns pattern (Fig S5), illustrating that  $\text{NO}_3^-$  anions in the interlayer of DI-LDH Ns are exchanged by MO during the intercalation process. Additionally, the O–H bands of both adsorbents shift after adsorption, indicating the hydrogen bonding interaction has formed between  $-\text{OH}$  of the LDH surface and the N or O atom of

MO [40]. From the discussion above, it could be concluded that the surface-interlayer-adsorption process happens on DI-LDH Ns because of its unique ultrathin  $\text{DS}^-$ -intercalated structure, while the adsorption of MO in DM-LDH Ns is merely the surface-adsorption process (Scheme 1).

This mechanism could well explain the tendency of the volcano curve (Fig. 5b) in Section 3.3.2, in which the adsorption efficiency of DI-LDH Ns exhibits an optimum value at  $\text{pH} = 9.0$ , exactly the point of zero charge of these  $\text{DS}^-$ -intercalated nanosheets (Fig. 5a). When the adsorbent surface is positively charged in weak acid to weak alkali condition, MO is easy to adsorb on its external surface quickly, which makes the sheets become negatively charged and partly impedes the dye from interlayer adsorption. And when DI-LDH Ns carries negative charges in a strong alkaline condition, the mutual exclusion between the electronegative laminates and the anionic dye impedes the adsorption process. Thus, DI-LDH Ns carrying fewer charges is favorable for more interlayer adsorption. In addition, it should be emphasized that the endothermic process taking place in DI-LDH Ns is mainly attributed to the intercalation process of MO, which is another marked difference between the surface-interlayer-adsorption and the surface-adsorption mechanism.

The content of adsorption was further demonstrated with TGA (Fig. 6c). Assuming the weight loss before  $100^\circ\text{C}$  (the first step) in TGA plot of MO/DI-LDH Ns is assigned to the desorption of physically adsorbed water, the weight loss between  $100^\circ\text{C}$  and  $700^\circ\text{C}$  could be attributed to the oxidation of organic components as well as the decomposition of residual small inorganic anions and hydroxide layers. The weight loss amount of MO/DI-LDH Ns is



Scheme 1. Adsorption mechanism of O-LDH, DM-LDH Ns and DI-LDH Ns.

calculated as 65.6% based on the dehydrated sample. This value is much larger than that of DI-LDH Ns of 40.1%, further proving a great quantity of MO are absorbed by this adsorbent. The theoretical weight loss percentage (%) of dehydrated MO/DI-LDH/Ns is further estimated by the following equation:

$$\text{Weight loss percentage (MO/DI - LDH Ns, \%)} = \frac{\text{Weight loss (DI - LDH Ns)} + \text{Weight loss (MO anion)}}{\text{Weight (DI - LDH Ns)} + \text{Weight (MO anion)}}$$

As has been fitted in adsorption isotherm (Table 3), the maximum adsorbed amount of MO molecules on hydrated DI-LDH Ns is 846.6 mg/g, i.e., 787.1 mg/g of MO anions. Thus, the adsorption quantity of MO anions on this dehydrated adsorbent would be 795.5 mg/g, corresponding to the weight loss percentage of 67.0% in dehydrated MO/DI-LDH/Ns. This value is close to the actual weight loss percentage (65.6%). The slight positive deviation might be ascribed to the ion-exchange of MO anions with the other anions such as  $\text{NO}_3^-$  during the adoption process (Fig S5).

What's more, as shown in Table 3, the adsorption amount per unit of surface area ( $q_s$ ,  $\text{mg/m}^2$ ) of DI-LDH Ns, DM-LDH Ns and O-LDH is 6.70, 3.39, and 8.51  $\text{mg/m}^2$ , respectively. Combined with the monolayer adsorption mechanism of the Langmuir model, the value of DM-LDH Ns is much smaller than that of O-LDH, indicating  $\text{DS}^-$  anions partly occupy the active sites on the adsorbent surface which prevents the further adsorption of MO. The ultrathin morphology of DM-LDH Ns with the higher external surface area plays the dominant role in its higher adsorption amount. The  $q_s$  value of DI-LDH Ns is larger than that of DM-LDH Ns owing to its interlayer adsorption, yet still smaller than O-LDH probably due to the partial occupation of  $\text{DS}^-$  on its surface. To summarize, it is the synergism of hydrogen bonding and electrostatic interaction in the surface-interlayer-adsorption process of DI-LDH Ns that endows its high adsorption performance in dye removal.

#### 4. Conclusion

In summary, a simple one-step surfactant-assisted hydrothermal method has been developed to prepare Mg-Al-LDH nanosheets with ultrathin morphology and tunable  $\text{DS}^-$  anions intercalated structure. It is an easy-operating and high-yielding method to prepare ultrathin organic-molecule-intercalated LDH without strict synthetic conditions to prevent  $\text{CO}_3^{2-}$  pollution. Furthermore, ultrathin  $\text{DS}^-$ -intercalated Mg-Al-LDH nanosheets have been successfully demonstrated as a rapid and high-effective adsorbent for removing dyes. The unique structural features of DI-LDH Ns endow its outstanding uptake capability ( $q_{\text{max}} = 846.6 \text{ mg/g}$  at 298 K) and quite short adsorbing equilibrium time (5 min) in MO removal. The sorption capacity of DI-LDH Ns increases as the temperature rises, and its adsorption isotherm follows the Langmuir equation. In addition, the surface-interlayer-adsorption mechanism of DI-LDH Ns has been summarized by characterizing the properties of the LDH nanosheets after dye adsorption with XRD, FT-IR and TGA. It is the unique characteristics of the ultrathin morphology with large surface area as well as the surfactant-intercalated structure that greatly increase its accessible active sites to promote the surface adsorption and intercalation of dye molecules. These results illustrate the advantage of the surfactant-intercalated Mg-Al-LDH with ultrathin nanosheet morphology and further point out a new protocol for developing competitive adsorbents for solving dye pollution.

#### CRedit authorship contribution statement

**Siqi Lei:** Conceptualization, Investigation, Data curation, Formal analysis, Writing - original draft, Visualization. **Sinong Wang:**

Resources, Conceptualization, Formal analysis, Visualization, Writing - review & editing, Project administration. **Boxu Gao:** Formal analysis, Validation, Writing - review & editing. **Yulu Zhan:** Investigation, Formal analysis, Data curation. **Qiancheng Zhao:** Investigation. **Shanshan Jin:** Investigation, Validation. **Guoxin Song:** Methodology. **Xinchun Lyu:** Methodology, Formal analysis, Project administration. **Yahong Zhang:** Resources, Formal analysis, Writing - review & editing. **Yi Tang:** Resources, Formal analysis, Writing - review & editing, Supervision.

#### Declaration of Competing Interest

The authors declare that they have no known competing financial interests or personal relationships that could have appeared to influence the work reported in this paper.

#### Acknowledgements

This work was supported by the National Major Research and Development Plan (Grant No. 2018YFA0209402), National Nature Science Foundation of China (Grant No.21703041, 21473037), and Shanghai Sailing Program (Grant No. 17YF1401100).

#### Appendix A. Supplementary data

Supplementary data to this article can be found online at <https://doi.org/10.1016/j.jcis.2020.05.050>.

#### References

- [1] S.F. Li, Removal of crystal violet from aqueous solution by sorption into semi-interpenetrated networks hydrogels constituted of poly(acrylic acid-acrylamide-methacrylate) and amylose, *Bioresour. Technol.* 101 (7) (2010) 2197–2202.
- [2] Z.R. Guo, Q. Chen, H.J. Gu, Z.F. He, W.Y. Xu, J.L. Zhang, Y.X. Liu, L.Y. Xiong, L.Z. Zheng, Y.J. Feng, Giant microgels with  $\text{CO}_2$ -Induced on-off, selective, and recyclable adsorption for anionic dyes, *ACS Appl. Mater. Interfaces* 44 (2018) 38073–38083.
- [3] R. Anliker, E.A. Clarke, The ecology and toxicology of synthetic organic pigments, *Chemosphere* 9 (10) (1980) 595–609.
- [4] A. Kausar, M. Iqbal, A. Javed, K. Aftab, Z.I.H. Nazli, H.N. Bhatti, S. Nouren, Dyes adsorption using clay and modified clay: a review, *J. Mol. Liq.* 256 (2018) 395–407.
- [5] Z. Yang, S.S. Ji, W. Gao, C. Zhang, L. Ren, W.W. Tjiu, Z. Zhang, J.S. Pan, T.X. Liu, Magnetic nanomaterial derived from graphene oxide/layered double hydroxide hybrid for efficient removal of methyl orange from aqueous solution, *J. Colloid Interface Sci.* 408 (2013) 25–32.
- [6] Y. Zhang, K.D. Li, J. Liao, Facile synthesis of reduced-graphene-oxide/rare-earth-metal-oxide aerogels as a highly efficient adsorbent for Rhodamine-B, *Appl. Surf. Sci.* 504 (2020) 144377.
- [7] A. Garg, M. Mainrai, V.K. Bulasara, S. Barman, Experimental investigation on adsorption of amido Black 10B dye onto zeolite synthesized from fly ash, *Chem. Eng. Commun.* 202 (1) (2015) 123–130.
- [8] M. Ghaedi, F. Karimi, B. Barazesh, R. Sahraei, A. Daneshfar, Removal of Reactive Orange 12 from aqueous solutions by adsorption on tin sulfide nanoparticle loaded on activated carbon, *J. Ind. Eng. Chem.* 19 (3) (2013) 756–763.
- [9] S.T. Yang, S. Chen, Y.L. Chang, A.N. Cao, Y.F. Liu, H.F. Wang, Removal of methylene blue from aqueous solution by graphene oxide, *J. Colloid Interface Sci.* 359 (1) (2011) 24–29.
- [10] J. Xiong, J. Di, W.S. Zhu, H.M. Li, Hexagonal boron nitride adsorbent: synthesis, performance tailoring and applications, *J. Energy Chem.* 40 (2020) 99–111.
- [11] L. Zhang, K.N. Hui, K.S. Hui, H. Lee, High-performance hybrid supercapacitor with 3D hierarchical porous flower-like layered double hydroxide grown on nickel foam as binder-free electrode, *J. Power Sources* 318 (2016) 76–85.
- [12] M. Dadwhal, M. Sahimi, T.T. Tsotsis, Adsorption isotherms of arsenic on conditioned layered double hydroxides in the presence of various competing ions, *Ind. Eng. Chem. Res.* 50 (4) (2011) 2220–2226.
- [13] G.D. Shi, C. Yu, Z.X. Fan, J.B. Li, M.J. Yuan, Graphdiyne-supported NiFe layered double hydroxide nanosheets as functional electrocatalysts for oxygen evolution, *ACS Appl. Mater. Interfaces* 11 (3) (2019) 2662–2669.
- [14] M. Gong, Y.G. Li, H.L. Wang, Y.Y. Liang, J.Z. Wu, J.G. Zhou, J. Wang, T. Regier, F. Wei, H.J. Dai, An advanced Ni-Fe layered double hydroxide electrocatalyst for water oxidation, *J. Am. Chem. Soc.* 135 (23) (2013) 8452–8455.
- [15] H. Chen, L.F. Hu, M. Chen, Y. Yan, L.M. Wu, Nickel-cobalt layered double hydroxide nanosheets for high-performance supercapacitor electrode materials, *Adv. Funct. Mater.* 24 (7) (2014) 934–942.

- [16] M.S. Usman, M.Z. Hussein, A.U. Kura, S. Fakurazi, M.J. Masarudin, F.F.A. Saad, Chlorogenic acid intercalated Gadolinium-Zinc/Aluminium layered double hydroxide and gold nanohybrid for MR imaging and drug delivery, *Mater. Chem. Phys.* 240 (2020) 122232.
- [17] Q. Wang, X.F. Wang, C.L. Shi, LDH Nanoflower lantern derived from ZIF-67 and its application for adsorptive removal of organics from water, *Ind. Eng. Chem. Res.* 57 (37) (2018) 12478–12484.
- [18] B. Zhang, Z.H. Dong, D.J. Sun, T. Wu, Y.J. Li, Enhanced adsorption capacity of dyes by surfactant-modified layered double hydroxides from aqueous solution, *J. Ind. Eng. Chem.* 49 (2017) 208–218.
- [19] W. Yao, S.J. Yu, J. Wang, Y.D. Zou, S.S. Lu, Y.J. Ai, N.S. Alharbi, A. Alsaedi, T. Hayat, X.K. Wang, Enhanced removal of methyl orange on calcined glycerol-modified nanocrystalline Mg/Al layered double hydroxides, *Chem. Eng. J.* 307 (2017) 476–486.
- [20] H.W. Pang, Y.H. Wu, X.X. Wang, B.W. Hu, X.K. Wang, Recent advances in composites of graphene and layered double hydroxides for water remediation: a review, *Chem.-Asian J.* 14 (15) (2019) 2542–2552.
- [21] Y.X. Chen, C. Jing, X. Zhang, D.B. Jiang, X.Y. Liu, B.Q. Dong, L. Feng, S.C. Li, Y.X. Zhang, Acid-salt treated CoAl layered double hydroxide nanosheets with enhanced adsorption capacity of methyl orange dye, *J. Colloid Interface Sci.* 548 (2019) 100–109.
- [22] F.R. Costa, A. Leuteritz, U. Wagenknecht, D. Jehnichen, L. Haussler, G. Heinrich, Intercalation of Mg-Al layered double hydroxide by anionic surfactants: preparation and characterization, *Appl. Clay Sci.* 38 (3–4) (2008) 153–164.
- [23] S.T. Lin, H.N. Tran, H.P. Chao, J.F. Lee, Layered double hydroxides intercalated with sulfur-containing organic solutes for efficient removal of cationic and oxyanionic metal ions, *Appl. Clay Sci.* 162 (2018) 443–453.
- [24] N. Iyi, K. Tamura, H. Yamada, One-pot synthesis of organophilic layered double hydroxides (LDHs) containing aliphatic carboxylates: extended “homogeneous precipitation” method, *J. Colloid Interface Sci.* 340 (1) (2009) 67–73.
- [25] M. Daud, A. Hai, F. Banat, M.B. Wazir, M. Habib, G. Bharath, M.A. Al-Harhi, A review on the recent advances, challenges and future aspect of layered double hydroxides (LDH) - containing hybrids as promising adsorbents for dyes removal, *J. Mol. Liq.* 288 (2019) 110989.
- [26] M. Zubair, M. Daud, G. McKay, F. Shehzad, M.A. Al-Harhi, Recent progress in layered double hydroxides (LDH)-containing hybrids as adsorbents for water remediation, *Appl. Clay Sci.* 143 (2017) 279–292.
- [27] M. Meyn, K. Beneke, G. Lagaly, Anion-exchange reactions of layered double hydroxides, *Inorg. Chem.* 29 (26) (1990) 5201–5207.
- [28] M. Meyn, K. Beneke, G. Lagaly, Anion-exchange reactions of hydroxy double salts, *Inorg. Chem.* 32 (7) (1993) 1209–1215.
- [29] A.A.A. Ahmed, Z.A. Talib, M.Z. Hussein, Influence of sodium dodecyl sulfate concentration on the photocatalytic activity and dielectric properties of intercalated sodium dodecyl sulfate into Zn-Cd-Al layered double hydroxide, *Mater. Res. Bull.* 62 (2015) 122–131.
- [30] P. Zhang, G.R. Qian, Z.P. Xu, H.S. Shi, X.X. Ruan, J. Yang, R.L. Frost, Effective adsorption of sodium dodecylsulfate (SDS) by hydrocalumite (CaAl-LDH-Cl) induced by self-dissolution and re-precipitation mechanism, *J. Colloid Interface Sci.* 367 (2012) 264–271.
- [31] F. Cavani, F. Trifiro, A. Vaccari, Hydroxalite-type anionic clays: preparation, properties and applications, *Catal. Today* 11 (2) (1991) 173–301.
- [32] J. Wang, D.J. Kang, X.L. Yu, M.F. Ge, Y.T. Chen, Synthesis and characterization of Mg-Fe-La trimetal composite as an adsorbent for fluoride removal, *Chem. Eng. J.* 264 (2015) 506–513.
- [33] M.L. Zhang, Q.F. Yao, C. Lu, Z.H. Li, W.X. Wang, Layered double hydroxide-carbon dot composite: High-performance adsorbent for removal of anionic organic dye, *ACS Appl. Mater. Interfaces* 6 (22) (2014) 20225–20233.
- [34] R. Hu, X.K. Wang, S.Y. Dai, D.D. Shao, T. Hayat, A. Alsaedi, Application of graphitic carbon nitride for the removal of Pb(II) and aniline from aqueous solutions, *Chem. Eng. J.* 260 (2015) 469–477.
- [35] Y.S. Ho, G. McKay, The kinetics of sorption of basic dyes from aqueous solution by sphagnum moss peat, *Can. J. Chem. Eng.* 76 (4) (1998) 822–827.
- [36] H. Freundlich, Concerning adsorption in solutions, *Zeitschrift Fur Physikalische Chemie-Stoichiometrie Und Verwandtschaftslehre* 57 (4) (1906) 385–470.
- [37] X.F. Zhang, L.Y. Ji, J. Wang, R.M. Li, Q. Liu, M.L. Zhang, L.H. Liu, Removal of uranium(VI) from aqueous solutions by magnetic Mg-Al layered double hydroxide intercalated with citrate: kinetic and thermodynamic investigation, *Colloids Surf. A* 414 (2012) 220–227.
- [38] M.E. Mahmoud, G.M. Nabil, N.M. El-Mallah, H.I. Bassiouny, S. Kumar, T.M. Abdel-Fattah, Kinetics, isotherm, and thermodynamic studies of the adsorption of reactive red 195 A dye from water by modified Switchgrass Biochar adsorbent, *J. Ind. Eng. Chem.* 37 (2016) 156–167.
- [39] X.X. Ruan, Y.H. Chen, H. Chen, G.R. Qian, R.L. Frost, Sorption behavior of methyl orange from aqueous solution on organic matter and reduced graphene oxides modified Ni-Cr layered double hydroxides, *Chem. Eng. J.* 297 (2016) 295–303.
- [40] Z.X. Jin, X.X. Wang, Y.B. Sun, Y.J. Ai, X.K. Wang, Adsorption of 4-n-Nonylphenol and Bisphenol-A on magnetic reduced graphene oxides: a combined experimental and theoretical studies, *Environ. Sci. Technol.* 49 (15) (2015) 9168–9175.
- [41] D. Chen, Y. Li, J. Zhang, J.Z. Zhou, Y. Guo, H. Liu, Magnetic Fe<sub>3</sub>O<sub>4</sub>/ZnCr-layered double hydroxide composite with enhanced adsorption and photocatalytic activity, *Chem. Eng. J.* 185 (2012) 120–126.
- [42] K. El Hassani, B.H. Beakou, D. Kalnina, E. Oukani, A. Anouar, Effect of morphological properties of layered double hydroxides on adsorption of azo dye Methyl Orange: a comparative study, *Appl. Clay Sci.* 140 (2017) 124–131.